

Normal-Branch Quasi-Periodic Oscillations during the High Intensity State of Cygnus X-2

Rudy Wijnands^{1*} & Michiel van der Klis²

¹Center for Space Research, MIT, 77 Massachusetts Avenue, Cambridge, MA 02139-4307, USA

²Astronomical Institute “Anton Pannekoek”, University of Amsterdam, Kruislaan 403, NL-1098 SJ Amsterdam, The Netherlands

27 October 2018

ABSTRACT

Using data obtained with the *Rossi X-ray Timing Explorer*, we report the detection of a 5 Hz quasi-periodic oscillation (QPO) in the bright low-mass X-ray binary and Z source Cygnus X-2 during high overall intensities (the high intensity state). This QPO was detected on the so-called normal branch and can be identified with the normal branch QPO or NBO. Our detection of the NBO is the first one during times when Cygnus X-2 was in the high intensity state. The rms amplitude of this QPO decreased from 2.8% between 2–3.1 keV to <1.9% between 5.0–6.5 keV. Above 6.5 keV, its amplitude rapidly increased to ~12% rms above 16 keV. The time lags of the QPO were consistent with being zero below 5 keV (compared to the 2–3.1 keV band), but they rapidly increased to ~70 ms (140°) around 10 keV, above which the time lags remained approximately constant near 70 ms. The photon energy dependencies of the rms amplitude and the time lags are very similar to those observed for the NBO with other satellites (*Ginga*, *EXOSAT*) at different (i.e. lower) intensity states.

Key words: accretion, accretion discs – stars: neutron – stars: individual: Cygnus X-2 – X-rays: stars

1 INTRODUCTION

Although the low-mass X-ray binary (LMXB) and Z source (Hasinger & van der Klis 1989) Cygnus X-2 is one of the best studied LMXBs, its complex behaviour is far from understood. On time-scales of hours to days, the source traces out its characteristic Z shape pattern in the X-ray colour-colour diagram (CD). The branches of this Z are called, from top to bottom, the horizontal branch (HB), the normal branch (NB), and the flaring branch (FB). On time-scales of weeks to months, the overall intensity varies smoothly by a factor of about 4 (see, e.g., Fig. 1). The exact morphology of the Z track and the position of this track in the CD (and hence the overall hardness of the X-ray spectrum) varies significantly when the overall intensity changes (see, e.g., Kuulkers, van der Klis, & Vaughan 1996 and Wijnands et al. 1997 for overviews of these changes). The first few months of the *Rossi X-ray Timing Explorer* (*RXTE*; Bradt, Rothschild, & Swank 1993) All Sky Monitor (ASM) data of Cygnus X-2 suggested an ~78 day period in the long-term variations (Wijnands, Kuulkers, & Smale 1996). Although this period is still one of the strongest periods, analyses of all *RXTE*/ASM data now available (up to 2000 October 9) show that the long-term variations are more complex than

only one single periodicity (see also Kong, Charles, & Kuulkers 1998 and Paul, Kitamoto, & Makino 2000).

The physical mechanism behind the long-term variations in Cyg X-2 is unknown. Several mechanisms have been proposed, such as variations in the mass accretion rate onto the neutron star, a precessing accretion disc, or a precessing neutron star (see Wijnands et al. 1997 and references therein for a discussion of these possible mechanisms). Although variations in the mass accretion rate are unlikely to cause the long-term variability (these variations are thought to produce the motion of Cyg X-2 along the Z track; see, e.g., Hasinger & van der Klis 1989, Kuulkers et al. 1996, and Wijnands et al. 1997), a precessing accretion disc or a precessing neutron star are still possible. Besides affecting the X-ray count rate and the X-ray spectrum, both mechanisms would most likely also affect the rapid X-ray variability, although it is unclear how exactly the variability would be affected. A detailed study of the rapid X-ray variability during different overall intensities might give new insights into the physics behind the long-term variability of Cyg X-2. However, such a detailed study has not yet been performed. Below we briefly list the results so far available.

On the HB, quasi-periodic oscillations (QPOs) between 15 and 55 Hz are observed (the horizontal branch QPOs or HBOs). These QPOs are also often observed on the upper part of the NB. A detailed comparison of the HBO prop-

* Chandra Fellow; Email: rudy@space.mit.edu

Table 1. Log of the *RXTE* observations of Cygnus X-2

Observation ID	Start (UT)	End (UT)	On source time (ks)
30418-01-01-00	1998 July 2 10:48	1998 July 2 14:30	8.2
30418-01-02-00	1998 July 3 11:37	1998 July 3 12:42	3.3
30418-01-02-01	1998 July 3 13:13	1998 July 3 14:15	3.7
30418-01-03-00	1998 July 4 11:38	1998 July 4 14:15	7.3
30418-01-04-00	1998 July 5 11:38	1998 July 5 14:14	7.3
30418-01-05-00	1998 July 6 09:07	1998 July 6 14:14	11.7

erties during different overall intensities (hereafter referred to as different intensity states) has not yet been made. Although Wijnands et al. (1997) reported that the HBO is always observed on the HB regardless of the overall intensity of Cygnus X-2, the HBO properties could differ in detail between different intensity states.

On the NB, QPOs with frequencies near 5 Hz can also be observed (the normal-branch oscillations or NBOs; sometimes observed simultaneous with the HBO). Also the NBO properties have not yet been compared between different intensity states, although Wijnands et al. (1997) did not detect the NBO (on the lower NB; with typical upper limits of <1% rms on the NBO amplitude) during the high intensity states observed using *Ginga* data of Cyg X-2. The NBOs were observed during lower intensity states.

Another type of QPO (with frequencies between 300 and 900 Hz) was recently discovered (Wijnands et al. 1998) in Cygnus X-2 when this source was on the HB during a medium intensity state: the kHz QPOs. These QPOs were not observable during a higher intensity state (Smale 1998) with upper limits which were smaller than the measured values.

Here, we report the first detection of a NBO in Cyg X-2 during a high intensity state demonstrating that this type of QPO is so far always observable regardless of the overall intensity of the source. The energy dependence of the rms amplitude and the time lags of this NBO are very similar to those observed during lower intensity states.

2 OBSERVATIONS AND ANALYSIS

Cygnus X-2 was observed by the *RXTE* proportional counter array (PCA; Jahoda et al. 1996) on several occasions between 1998 June 2–7 for a total of ~ 42 ksec (see Table 1 for a log of the observations). Data were obtained in 129 photon energy channels (covering 2–60 keV) with a time resolution of 16 s. Simultaneous data were obtained in two “Single Bit” modes (one energy channel each; time resolution of 128 μ s; energy range 2–5.0 and 5.0–13.0 keV), one “Event” mode (64 channels; 16 μ s; 13.0–60 keV), and one “Binned” mode (16 channels; 2 ms; 2–13.0 keV). We used the 16 s data to create the CD and the hardness-intensity diagram (HID; see the caption of Fig. 3 for the energy bands used to calculate the colours). We used the Single Bit modes and the Event modes to create 1/16–2048 Hz power spectra to study the rapid X-ray variability above 100 Hz (i.e., to search for kHz QPOs); we used the Binned and the Event modes to create 1/16–256 Hz power spectra and cross spectra to study the

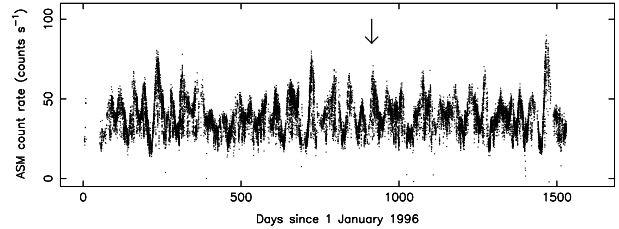


Figure 1. The *RXTE* All Sky Monitor light curve (1.3–12.1 keV) of Cygnus X-2 clearly showing the long-term X-ray variations. The arrow indicates when the observations of Cygnus X-2 were taken. The errors on the count rates are typical 3%–7%.

rapid X-ray variability below 100 Hz (i.e., to study the NBO and HBO). The strengths of the power spectral components are all given for the energy range 2–60 keV, unless otherwise noted.

3 RESULTS

Figure 1 shows the *RXTE*/ASM light curve of Cyg X-2 clearly showing the long-term X-ray variations. During the observations presented here, Cygnus X-2 was at high count rates. The *RXTE*/ASM count rates were approximately 60 counts s^{-1} (Fig. 2). The upper envelope of the ASM light curves in Figures 1 and 2 corresponds to epochs during which Cyg X-2 was on the NB; the short-lasting “drop-outs” from this upper envelope are excursions into the HB and the FB. These excursions do not define a lower envelope demonstrating that the overall intensity of Cyg X-2 is mainly defined by the count rate on the NB.

The CD and HID of the data are shown in Figure 3. In both diagrams, clear horizontal and normal branches are visible. The FB is not clearly visible in the CD (only as a broadening of the lower part of the normal branch) but in the HID an extended FB is present. The count rate decreased when Cygnus X-2 entered the FB. We selected the power spectra based on the position of the source on the track in the HID. The HID was used instead of the CD because by using the HID it was possible to disentangle the power spectra corresponding to the lower part of the NB and those corresponding to the FB.

In Figure 4, typical 2–60 keV power spectra are shown for different positions of the source on the Z track. On the HB, clear HBOs, their second harmonics, and strong (8%–10% rms) band-limited noise (the Z source low-frequency noise or LFN; Fig. 4a) were present. The frequency of the

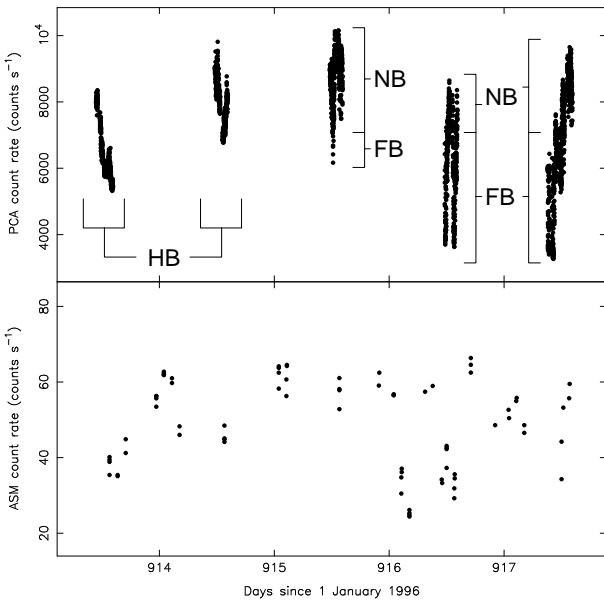


Figure 2. The *RXTE*/PCA light curve (2.0–16.0 keV) (*top panel*) and the All Sky Monitor light curve (1.3–12.1 keV) (*bottom panel*) at the time of the observations of Cygnus X-2. In the *top panel*, it is indicated on which branch the source was during the *RXTE*/PCA observations. The errors on the PCA and the ASM count rates are typical 0.3%–0.5% and 3%–7%, respectively.

HBO was ~ 30 Hz at the left end of the HB and increased smoothly to 49 Hz at the right end (see also Fig. 3*b*). The rms amplitude of the HBO at the left end of the HB was 5% and decreased to 4% when the source moved slightly to the right on the HB. The amplitude of the HBO on the rest of the HB stayed approximately constant at 4% rms. The FWHM of the HBO was 5 Hz at the left end of the HB and increased to 20 Hz when the source moved to the right end. Together with the HBO, its second harmonic could be detected from the left end up to halfway the HB, with an rms amplitude decreasing from 4.4% to 2.6% and a FWHM increasing from 24 to 36 Hz.

On the upper part of the observed normal branch (Fig. 4*b*), the HBO was still visible around 55 Hz (with an rms amplitude of 2%–3% and a FWHM of 20–30 Hz) together with a noise component below 1 Hz following a power law (the Z source very-low frequency noise or VLFN) and a peaked noise component near 5 Hz. Further down the NB and at the beginning of the FB (Fig. 4*c*), no QPOs were present, but the VLFN still was, together with a weak (several percent) noise component following a cutoff power law (cutoff frequency near 10 Hz; probably the Z source high-frequency noise or HFN). On the left end of the FB only the VLFN remained (Fig. 4*d*).

So, when using power spectra created for the total *RXTE*/PCA photon energy range (2–60 keV), no NBO were detected on the NB. However, when we examined the peaked noise component on the upper part of the observed NB (Fig. 4*b*) in more detail and in different energy ranges, a clear QPO around 5 Hz emerged. Figure 5 shows the power spectra corresponding to the upper normal branch but at different energies. The power spectrum in Figure 5*a* is the same as the one presented in Figure 4*b*, although now plot-

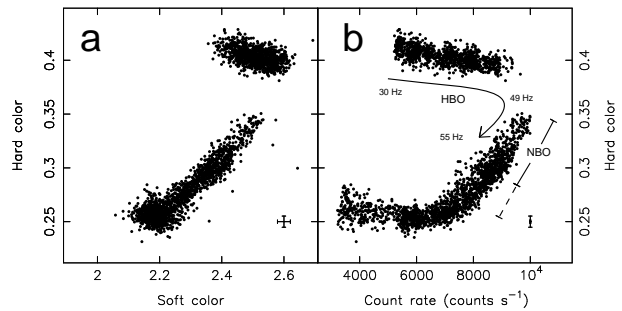


Figure 3. Colour-colour diagram (*a*) and hardness-intensity diagram (*b*) of Cygnus X-2. The soft colour is the count rate ratio between 3.5–6.4 and 2.0–3.5 keV, the hard colour that between 9.7–16.0 and 6.4–9.7 keV, and the count rate is in the energy range 2.0–16.0 keV. All points are 16 s averages. In (*b*) it is indicated when the HBO and the NBO were present in the data and how the frequency of the HBO changed (indicated by the arrow). The solid line labelled NBO indicates where the FWHM of the NBO was smaller than 5 Hz. All the data corresponding to this part of the Z track were used to calculate the energy dependence of the rms amplitude and the time lags of the NBO. The dashed line indicates where the FWHM increased to 7–13 Hz. Typical error bars on the colours and the intensity are indicated in the lower right corners of the diagrams.

ted with the power axis in linear scale in order to show the QPO more clearly. Figures 5*b* to *d* show the corresponding power spectra at different energies. At energies above 7.9 keV a very significant (29σ) QPO is clearly visible with a frequency of $5.37^{+0.08}_{-0.03}$ Hz, a FWHM of 4.4 ± 0.2 Hz, and an rms amplitude (7.9–60 keV) of $6.7\% \pm 0.1\%$. Note that the FWHM of the QPO is such that according to the usual criterion for a noise component to be called a QPO (the ratio of the FWHM to the frequency is < 0.5), this NBO was not truly a QPO. However, below we will use the term QPO for this peaked noise feature. By comparing Figures 5*a* and *d*, it is clear that this QPO is only visible as a broad peaked noise component near 5 Hz when combining the data of the whole *RXTE*/PCA energy range. The QPO was also visible at low (< 5 keV) photon energies (Fig. 5*b*), but not at energies between 5.0 and 6.4 keV.

After discovering the NBO at high photon energies, we reexamined all the power spectra corresponding to the different locations of the source on the Z track. We used the 7.9–60 keV energy range instead of the 2–60 keV one. The 7.9–60 keV power spectra on the horizontal branch were very similar to those in the 2–60 keV band. As said above, on the upper part of the observed normal branch a broad NBO was now clearly visible. The frequency (5.4 Hz), the FWHM (4 Hz), and the rms amplitude (7%) of the NBO did not change significantly when the source moved down the NB. Halfway down the NB, the QPO became much broader (with a FWHM of 7–13 Hz) and the NBO decreased slightly in amplitude (to 5%–6% rms). On the lower part of the NB (near the NB-FB vertex), the NBO could not be detected anymore with upper limits on the rms amplitude of 3%–4% (see also Fig. 3*b* for the region where the NBO could be detected). At the NB-FB vertex and on the FB the 7.9–60 keV power spectra were very similar to the 2–60 keV power spectra.

Figure 6*a* shows the count rate in the energy bands used

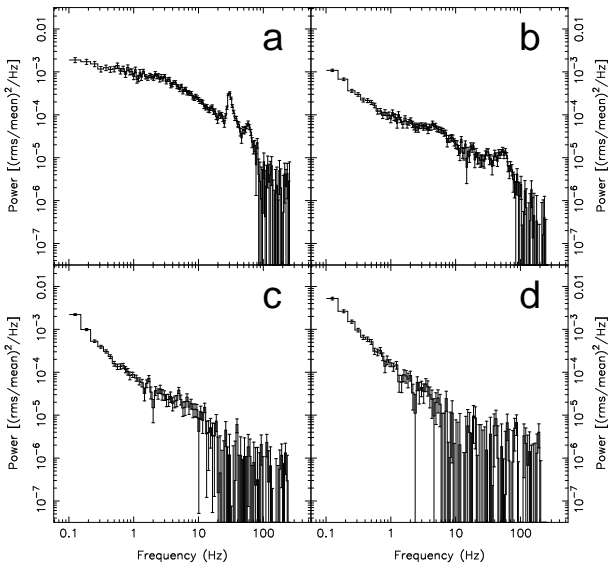


Figure 4. Typical power spectra for the full 2–60 keV energy range of Cygnus X-2 on: (a) the horizontal branch, (b) the upper part of the observed normal branch, (c) the normal-flaring branch vertex, and (d) the end of the flaring branch. The Poisson level has been subtracted.

to calculate the rms amplitude of the NBO. The rms amplitude of the NBO as a function of photon energy is plotted in Figure 6b. In order to calculate these rms amplitudes, we only used the data of the upper part of the observed NB for which the NBO had a FWHM which was lower than 5 Hz (see also Fig. 3b). The NBO decreased from about 3% rms at the lowest energies to <2% rms between 5 and 6.4 keV. Above 6.4 keV, the strength of the NBO rapidly increased to 10% at 15 keV. At higher energies the strength seemed to level off, although a firm conclusion cannot be made.

For the same data, we determined the time lags of the NBO between the different energy bands. In order to calculate the time lags of the NBO, we calculated the lags in the 4.4 Hz interval (corresponding to the FWHM of the NBO) centred on the peak frequency of the QPO (5.37 Hz). We subtracted the average cross-vector between 80 and 250 Hz in order to minimize the dead-time effects on the lags induced by Poisson fluctuations (see van der Klis et al. 1987). The resulted time lags are presented in Figure 6c. We used the 2–3.1 keV energy band as reference band. The time lags between this reference band and the bands below 5 keV were consistent with zero. Above 5 keV, the time lags increase rapidly to ~ 70 ms for energies between 8 and 9 keV. At higher energies, the time lags remained constant near 70 ms. This means that the hard photons lag the soft photons by about 70 ms (2.4 radians or 140°).

We searched for kHz QPOs in the total energy band and in the energy range 5.0–60 keV (as used by Wijnands et al. 1998 when kHz QPOs were present in Cyg X-2). None were found with typical (assuming a FWHM of 150 Hz) 95% confidence upper limits of 2%–3% (1%–2%) on the HB, 2%–3% (1%–1.5%) on the NB, and 2.5%–3.5% (1.5%–2.0%) on the FB in the energy range 5.0–60 keV (the limits enclosed within parentheses are for the total *RXTE/PCA* energy range). Two X-ray bursts were observed. We searched

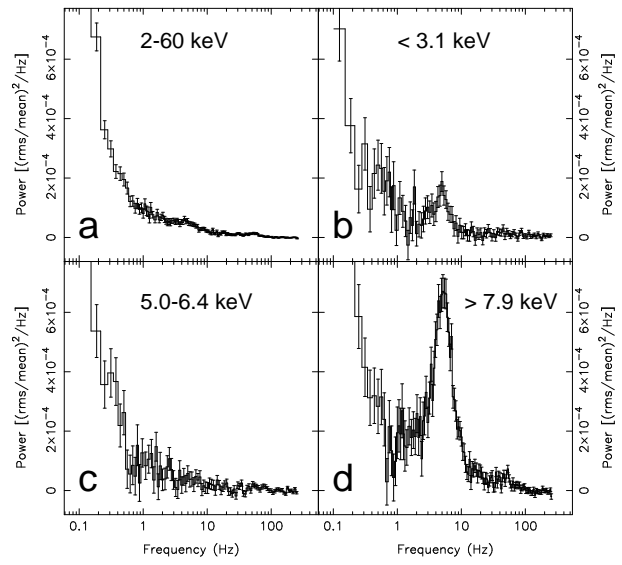


Figure 5. Typical power spectra of Cygnus X-2, when the source was on the upper part of our observed normal branch, in different energy ranges: (a) 2–60 keV, (b) below 3.1 keV, (c) 5.0–6.4 keV, and (d) above 7.9 keV. The Poisson level has been subtracted. The 2–60 keV power spectrum (a) is the same as shown in Fig. 4b, but now with the power axis plotted linear.

for (nearly) coherent oscillations, as reported in several other LMXBs (e.g., Strohmayer et al. 1996; Smith, Morgan, & Bradt 1997), but none were found with upper limits of 4%–7% (2–60 keV).

4 DISCUSSION

We have detected the NBO on the upper part of our observed normal branch of Cygnus X-2 when this source was at relative high overall intensities (Fig. 1). The shape of the Z track in the CD and the HID was very similar to those observed with *Ginga* for Cygnus X-2 in the high intensity state (Wijnands et al. 1997; i.e., compare their Fig. 1 with our Fig. 3). Therefore, we conclude that Cygnus X-2 was in a high overall intensity state during the observations reported here. This conclusion is strengthened by the fact that our power spectra on the lower normal branch resemble those obtained by Wijnands et al. (1997) in the high intensity state, especially the non-detection of the NBO on the lower part of the NB (compare their Figs. 8g–i with our Figs. 4c and d). Wijnands et al. (1997) were unable to search for the NBO further upwards on the NB (the middle and upper part of the NB) due to the fact that they did not have enough high time resolution data at those positions on the Z track. Our *RXTE/PCA* data are the first high time resolution data available on the middle and upper part of the NB of Cygnus X-2 during the high intensity state.

Our first clear detection of the NBO in the high intensity state of Cygnus X-2 shows that all power spectral components which are observed below 100 Hz in Cygnus X-2 are present at high overall intensities. So far, the only clear difference in the timing properties of Cygnus X-2 during different intensity states are the detection of the kHz QPOs on the HB during a medium intensity state (Wijnands et al.

1997) but not during high intensity states (Smale 1998 and this paper). More detections of the kHz QPOs in Cygnus X-2 are needed in order to determine the exact reason(s) why the kHz QPOs are only present during preferred intensity states.

Wijnands et al. (1997) pointed out that a precessing accretion disc, one of the proposed explanations for the long-term X-ray variations of Cyg X-2 (e.g., Kuulkers et al. 1996; Wijnands et al. 1996), could not easily account for the non-detection of the NBO during the high intensity state. Our detection of the NBO during this state now shows that the arguments used by Wijnands et al. (1997) are not valid any more when only considering the NBO. However, when also considering the kHz QPOs, it is clear that the precessing accretion disc model has still difficulties explaining the difference in rapid X-ray timing variability (i.e., the kHz QPOs) when Cyg X-2 is at different intensity states. In the precessing accretion disc scenario, it is possible that more matter is blocking the emission region during low intensity states (hence the lower overall intensity) than during high intensity states. If this the case then during these low states, the amplitudes of the kHz QPOs should be significantly lower than in the high states due to more scattering of the radiation. However, we see exactly the opposite: no kHz QPOs are detected during the high intensity state. It is also possible that the precession of the accretion disc causes changes in the projected area of the inner disc which could result in the different intensity states. However, then the kHz QPOs would be expected in all intensity states, i.e., also during the high intensity state. The non-detections of the kHz QPOs during the high intensity state constitute a serious problem for the precessing accretion disc model.

We now compare our results obtained for the NBO to those which have been published previously. The best cases to compare our results with are the *Ginga* June 1987 observations of Cygnus X-2 reported by Mitsuda & Dotani (1989; see also Wijnands et al. 1997) and the *EXOSAT* November 14/15 1985 observations which are reported by Dieters et al. (2000; see also Hasinger et al. 1985,1987). Wijnands et al. (1997) classified the intensity state of Cyg X-2 during the *Ginga* observations as intermediate between the high and the medium intensity state. Kuulkers et al (1996) classified the state during the *EXOSAT* observations as the medium state (see Wijnands et al. 1997 for the classification of the different states of Cygnus X-2).

During the *Ginga* observations (Mitsuda & Dotani 1989; Wijnands et al. 1997) and the *EXOSAT* observations (Dieters et al. 2000), the NBO was best visible on the middle part of the NB. The NBO was much less clear on the upper and lower parts of the NB (although excess power on top of a power-law function was present near 5 Hz). The exact position on the Z track where the NBO is present during those observations is very similar to the positions on the track where we detect the NBO. Although we detected the NBO up to the upper most part of our observed NB and Mitsuda & Dotani (1989) and Dieters et al. (2000) did not detect the NBO on the upper part of their observed NB, this difference is most likely due to the fact that we did not observe the NB all the way to the HB/NB vertex (see Fig. 3b) and most likely they did. If we would have observed the NB all the way to the HB/NB vertex most likely we would not have detected the NBO either on this part of the Z track.

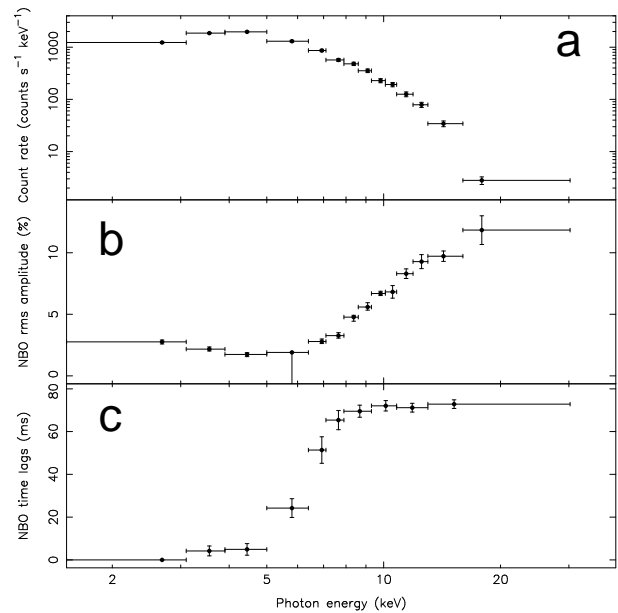


Figure 6. The count rate of the upper part of the observed NB (a), the rms amplitude of the NBO (b), and the time lags of the photon energy range from the averaged mean photon energy in the energy channels to the boundary of these channels.

Wijnands et al. (1997) also reported that the NBO was best visible at the middle of the NB during the medium state and that it tends to get broader when the source moves further down the NB. The energy dependence and time lags of our NBO are also nearly identical to those obtained for the NBO by Mitsuda & Dotani (1989) and Dieters et al. (2000). This indicates that the physical mechanism behind the long-term variation of the X-ray flux of Cygnus X-2 does not significantly affects the properties of the NBO.

From the presently available results, we conclude that so far no significant difference is present in the NBO properties during the high intensity state of Cygnus X-2 and during its intermediate and medium intensity state. Recently, Kuulkers, Wijnands, & van der Klis (1999) reported on *RXTE* observations of Cyg X-2 when this source was in a very low intensity state. No NBOs were detected. However, no complete Z track was traced out during these observations but most likely only the lower part of the NB and part of the FB. It is possible that when a complete Z track would have been traced out, the NBO would have been present at the middle part or upper part of the NB.

To explain the NBO in Z sources, it has been proposed that, when those sources are accreting close to the Eddington accretion limit, part of the accretion will occur in an approximately spherical radial inflow. In this radial flow a radiation pressure feed-back loop can be set up that causes 5–7 Hz oscillations in the optical depth of the flow (Fortner et al. 1989; Lamb 1989; Miller & Lamb 1992). This radiation-hydrodynamic model is able to explain the combination of the minimum in the rms amplitude spectrum of the NBO and the ~ 140 – 150° phase shift in the phase lags at the same photon energy (Miller & Lamb 1992). Miller & Lamb (1992) used the results reported by Mitsuda & Dotani (1989) to constrain their model. Because our results are so similar to

those published by Mitsuda & Dotani (1989), we are unable to constrain this radiation-hydrodynamic model further. In order to constrain this model, data are needed with a higher energy resolution than our *RXTE*/PCA data and/or data have to be obtained for the energy range below 3 keV, a region which we are unable to probe with our *RXTE*/PCA data. However, it has already been showed that this model cannot easily explain the differences in the NBO properties observed for Cyg X-2 and those observed for GX 5-1 and Sco X-1 (see, e.g., Dieters et al. 2000).

The recent discovery of a QPO near 7 Hz in the atoll source 4U 1820-30 (Wijnands, van der Klis, & Rijkhorst 1999) might even impose a more serious problem to all NBO models. The properties of this QPO in 4U 1820-30 (i.e., its frequency and its presence only at the highest observed mass accretion rates in this source) are similar to the NBO in the Z sources. However, if indeed these QPOs are the same phenomenon, then the models explaining the NBO in Z sources which require near-Eddington mass accretion rate, will not hold because the highest mass accretion rate observed in 4U 1820-30 (i.e., the accretion rate at the time of the 7 Hz QPO) is significantly lower than the critical Eddington mass accretion rate. This is not only true for the radiation-hydrodynamic model of Fortner et al. (1989), but also for alternative models, such as the sound wave model of Alpar et al. (1992). Clearly, the NBO models have to be significantly adjusted in order to explain all NBO properties and to explain the similarities between the NBO and the 7 Hz QPO in 4U 1820-30.

ACKNOWLEDGMENTS

This work was supported in part by the Netherlands Foundation for Research in Astronomy (ASTRON) grant 781-76-017, by the Netherlands Research School for Astronomy (NOVA), and the NWO Spinoza grant 08-0 to E. P. J. van den Heuvel. Support for this work was provided by the NASA through the Chandra Postdoctoral Fellowship grant number PF9-10010 awarded by the Chandra X-ray Center, which is operated by the Smithsonian Astrophysical Observatory for NASA under contract NAS8-39073. This research has made use of data obtained through the High Energy Astrophysics Science Archive Research Center Online Service, provided by the NASA/Goddard Space Flight Center.

REFERENCES

Alpar M.A., Hasinger G., Shaham J., Yancopoulos S., 1992, *A&A*, 257, 627
 Bradt H.V., Rothschild R.E., Swank J.H., 1993, *A&AS*, 97, 355
 Dieters S.W., Vaughan B.A., Kuulkers E., Lamb F.K., van der Klis M., 2000, *A&A*, 353, 203
 Fortner B., Lamb F.K., Miller G.S., 1989, *Nature*, 342, 775
 Hasinger G., Langmeier A., Sztajno M., Pietsch W., Gottwald M., 1985, *IAUC* 4153
 Hasinger G., in Helfand D.J., Huang J.-H. (eds) 1987 “The Origin and Evolution of Neutron Stars”, *IAU Symposium* 125, p. 333
 Hasinger G., & van der Klis M. 1989, *A&A*, 225, 79
 Jahoda K., Swank J.H., Giles A.B., Stark M.J., Strohmayer T., Zhang W., Morgan E.H., 1996, *SPIE*, 2808, 59
 Kong A.K.H., Charles P.A., Kuulkers E., 1998, *NewA* 3, 301

Kuulkers E., van der Klis M., Vaughan B.A., 1996, *A&A*, 311, 197
 Kuulkers E., Wijnands R., van der Klis M., 1999, *MNRAS*, 308, 485
 Lamb F.K., 1989, in Proc. 23 rd ESLAB Symp. on “Two Topics in X-ray Astronomy”, Bologna, Italy, 13-20 September 1989 (ESA SP-296), p. 215
 Miller G.S. & Lamb F.K., 1992, *ApJ*, 388, 541
 Mitsuda K., Dotani T., 1989, *PASJ* 41, 531
 Paul B., Kitamoto S., Makino F., 2000, *ApJ* 528, 410
 Smale A.P., 1998, *ApJ* 498, L141
 Smith D.A., Morgan E.H., Bradt H., 1997, *ApJ* 479, L137
 Strohmayer T.E., Zhang W., Swank J.H., Smale A., Titarchuk L., Day C., Lee U., 1996, *ApJ* 469, L9
 van der Klis M., Hasinger G., Stella L., Langmeier A, van Paradijs J., Lewin W.H.G., 1987, *ApJ* 319, L13
 Wijnands R.A.D., Kuulkers E., Smale A.P., 1996, *ApJ* 473, L45
 Wijnands R., van der Klis M., Kuulkers E., Asai K., Hasinger G., 1997, *A&A*, 323, 399
 Wijnands R., et al. 1998, *ApJ* 493, L87
 Wijnands R., van der Klis M., & Rijkhorst E.-J., 1999, *ApJ*, 512, L39